Supporting Information

Moscoso et al. 10.1073/pnas.1016113108

SI Materials and Methods

Purification, sample preparation, and cryoelectron microscopy of o-gp140ΔV2TV1 was performed as follows. Recombinant gp140 was expressed in a CHO cell line and isolated to 95% purity using a four step chromatography purification regime, with a *Galanthus nivalis* agglutinin lectin column to capture the Env construct, followed by a diethylaminoethyl column and a ceramic hydroxyapatite column, respectively, to capture contaminating proteins while Env flowed through, and concluding with size exclusion chromatography to isolate the trimeric form. Samples were prepared on holey carbon grids with a solution concentration of 0.1 mg/mL. The initial concentration of 0.2 mg/mL was halved when it was observed that some micrographs had areas of dense protein concentration not amenable to particle selection. Solutions of gp140 were diluted with Tris buffer (20 mM, pH 7.9) and 50 mM NaCl was added. To elicit the liganded conformation, gp140 was incubated overnight at 4 °C with CD4m in excess concentration.

Samples were imaged using a JEOL 2100F field emission electron microscope at 200 kV, with an electron dose of approximately 15 $e^{-}/Å^{2}$ (1, 2). A total of 101 micrographs for the unliganded state and 46 micrographs for the liganded state (Fig. S3*A* and *B*) were recorded at 80,000× magnification and used for single particle reconstruction via the EMAN software package (3). Roughly 4,500 individual native particle images and approximately 2,700 particle images of the liganded state were selected (Figs. S4 and S5).

1. Buchbinder SP, et al. (2008) Efficacy assessment of a cell-mediated immunity HIV-1 vaccine (the Step Study): A double-blind, randomised, placebo-controlled, test-of-concept trial. *Lancet* 372:1881–1893.
2. Kawano MA, et al. (2009) Calcium bridge triggers capsid disassembly in the cell entry process of simian virus 40. *J Biol Chem* 284:34703–34712.
3. Ludtke SJ, Baldwin PR, Chiu W (1999) EMAN: Semiautomated software for high-resolution single-particle reconstructions. *J Struct Biol* 12:82–97.

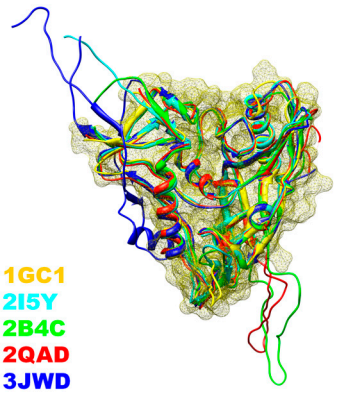

RMSD between 1GC1 and other gp120 coordinates

PDB	RMSD	Coordinate contents	Newly resolved regions
2I5Y	1.86	gp120-CD4m-17b	
2B4C	1.97	gp120-sCD4-X5	V3 loop
2QAD	1.76	gp120-sCD4-412D	
3JWD	1.52	gp120-sCD4-48D	N- and C-termini
1GC1		gp120-sCD4-17b	

Fig. S1. Structural comparison of selected existing HIV-1 gp120 coordinates. X-ray crystallographic coordinates of gp120 in complex with various ligands structurally matched using least-squares fitting. (*Left*) Four sets of gp120 coordinates were fitted to the earliest set of gp120 coordinates (PDB 1GC1). (*Right*) The table indicates the root mean square deviation (rmsd) between PDB 2I5Y, 2B4C, 2QAD, and 3JWD. As shown, the rmsd between 1GC1 and the other gp120 coordinates is consistently below 2 Å, thus giving similar results in docking.

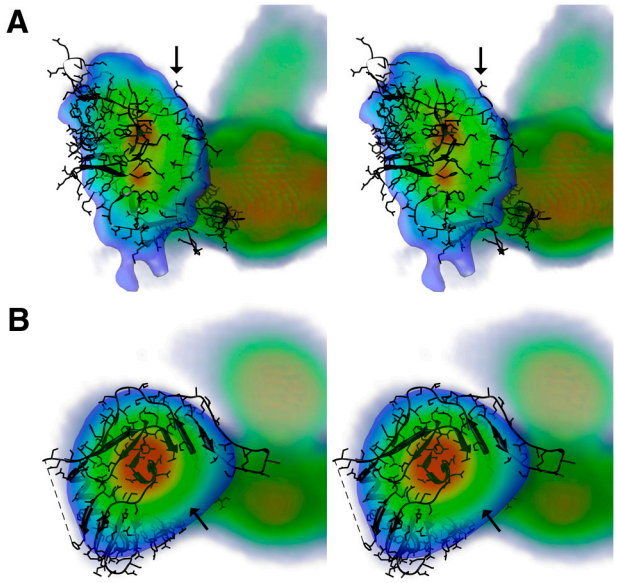

Fig. S2. Segmentation of gp140 in unliganded and liganded states viewed as stereo pairs. (*A*) Stereo pair of volume rendered unliganded gp140 docked with unliganded simian immunodeficiency virus gp120 in an oblique view with segmentation slice reveals areas of higher density (in red) compared to areas of lower density (in yellow, green, and blue). Arrow is pointing at the likely orientation of CD4 as it binds to the CD4-binding residues. (*B*) Stereo pair of volume rendered CD4m-bound gp140 in an oblique view with segmentation slice reveals a uniform area of high density. Arrow points to the location of the CD4 binding site subsequent to rotation of gp120 as described in Fig. 2.

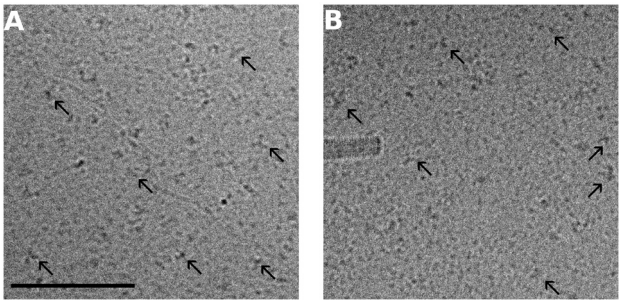

Fig. S3. Raw cryoelectron micrographs of unliganded and CD4m-liganded gp140. (*A*) Detail of cryo-EM micrograph of native, unliganded gp140 taken with a JEOL-2100F electron microscope at 200 kV. Defocus values ranged from 3.5 to 6 μm. Arrows point to sample raw trimer images. (*B*) Detail of cryo-EM micrograph of liganded gp140, taken under same conditions as in *A*. Arrows point to sample raw trimer images. Defocus values ranged from 3 to 6 μm. Scale bar = 100 nm for panel *A*, same scale in panel *B*.

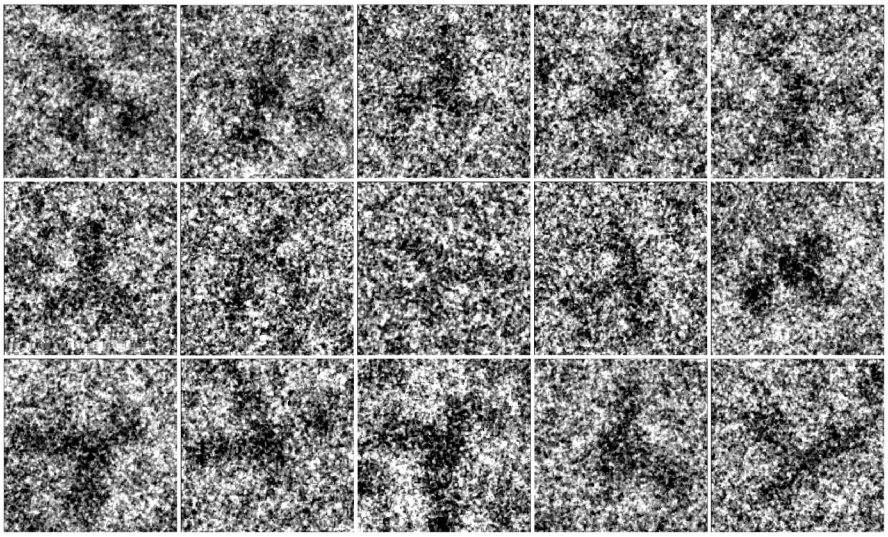

Fig. S4. Sample raw unliganded gp140 trimer images. Cryoelectron micrograph boxed particles displaying unliganded gp140. As evident from the images, gp140 is in a fan-blade motif with the gp120 subunits extending from the central stalk of gp41. Note the almost contiguous interface between gp120 and gp41, suggesting close association between these subunits.

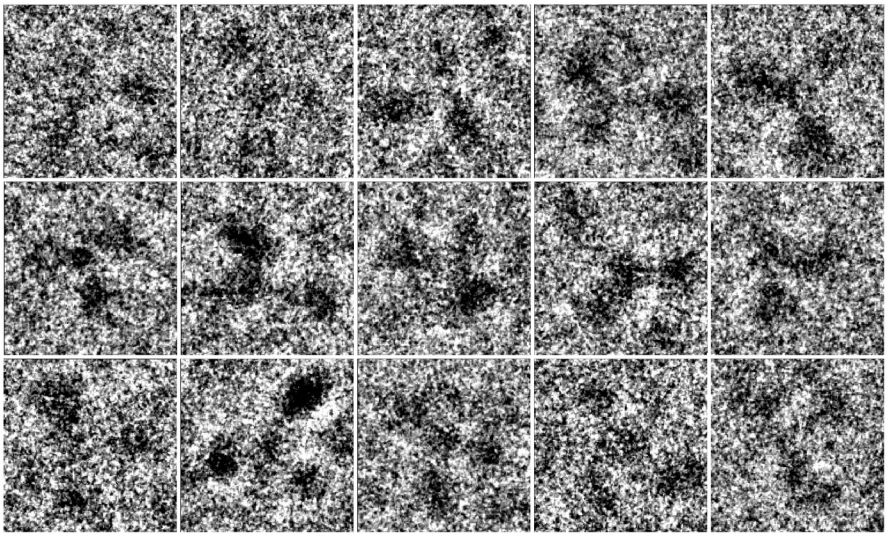

Fig. S5. Sample raw CD4m-bound gp140 trimer images. Cryoelectron micrograph boxed particles displaying CD4m-liganded gp140. The boxed particles clearly show a diminished interface between the gp120 subunits and the central gp41 stalk. Such a decreased contact with gp41 could trigger the conformational changes required to expose the gp41 N-terminal hydrophobic fusion peptide, priming it for insertion into the host membrane and initiating membrane fusion.

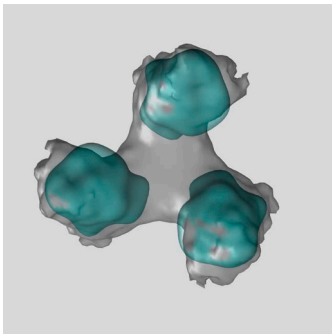

Movie S1. Morph between unliganded and liganded gp140 conformations reveals quaternary movements. Animation depicting the native, unliganded gp140 structure morphing into the CD4m-liganded gp140 structure. Docked within the trimer density maps are densities derived from docked coordinates; these were also morphed from unliganded simian immunodeficiency virus gp120 (PDB 2BF1) to CD4-bound HIV-1 gp120 (PDB 1GC1). One observation evident from the morphing is the tilt away from the threefold axis, which likely juxtaposes the host membrane with the threefold axis. Another observation is that of the subunit rotation, which would expose the coreceptor binding site and further weaken the gp120–gp41 interface. The sites of glycosylation (labeled) correspond to the outer edge of each trimer blade, whereas the approximate site of the V2 loop (labeled) is oriented toward the adjacent counterclockwise gp120 subunit. A still image of the movie at the start of the animation (in the unliganded state) was also provided.

Movie S1 (AVI)